Supporting Information

Uncovering the prominent role of metal ions in octahedral versus tetrahedral sites of cobalt-zinc oxide catalysts for efficient oxidation of water

Prashanth W. Menezes,[a] Arindam Indra,[a] Arno Bergmann,[b] Petko Chernev,[c] Carsten Walter,[a] Holger Dau,*[c] Peter Strasser*[b] and Matthias Driess*[a]

[a] Department of Chemistry: Metalorganics and Inorganic Materials, Technische Universität Berlin, Straße des 17 Juni 135, Sekr. C2, 10623 Berlin, Germany

[b] Department of Chemistry, The Electrochemical Energy, Catalysis, and Materials Science Group, Technische Universität Berlin, Straße des 17 Juni 124, Sekr. TC3, 10623 Berlin, Germany

[c] Fachbereich Physik, Freie Universität Berlin, Arnimallee 14, 14195 Berlin, Germany

Chemicals

All chemical reagents were used as received without any further purification and deionized water was used throughout the experiment. Commercially available cobalt (II) acetate tetrahydrate ($Co(CH_3COO)_2{\cdot}4H_2O$) and zinc(II) acetate dihydrate ($Co(CH_3COO)_2{\cdot}2H_2O$) were purchased from Alfa Aesar whereas ammonium sulfate $(NH_4)_2SO_4$ and ammonium bicarbonate (NH_4HCO_3) were procured from Sigma Aldrich.

Instrumental

Powder X-Ray Diffraction (PXRD) patterns were recorded on a Bruker AXS D8 advanced automatic diffractometer equipped with a position sensitive detector (PSD) and a curved germanium (111*)* primary monochromator using Cu *Kα* (λ = 1.5418 Å) radiation. The PXRD profiles were collected between $5° < 2\theta < 80°$. The structural models were drawn with the program DIAMOND version 3.0. The chemical composition of the precursors and oxides were confirmed by Inductively Coupled Plasma Atomic Emission Spectroscopy (ICP-AES) on a Thermo Jarrell Ash Trace Scan analyzer. Scanning Electron Microscopy (SEM) was performed on a LEO DSM 982 microscope integrated with EDX (EDAX, Appollo XPP). Data handling and analyses were achieved with the software package EDAX. Transmission Electron Microscopy (TEM) was carried out on a FEI Tecnai G^2 20 S-TWIN transmission electron microscope (FEI Company, Eindhoven, Netherlands) equipped with a LaB_6-source at 200 kV acceleration voltage.

Energy Dispersive X-ray (EDX) analysis were accomplished with an EDAX r-TEM SUTW detector (Si (Li)-detector) and the images were recorded with a GATAN MS794 P CCD-camera. The SEM and TEM experiments were performed at the Zentrum für Elektronenmikroskopie (ZELMI) of the TU Berlin. Fourier transform infrared spectroscopy (FTIR) was studied using a BIORAD FTS 6000 FTIR spectrometer under attenuated total reflection (ATR) setup. The data were recorded in the range of 400–4000 cm^{-1} with the average of 64 scans at 4 cm^{-1} resolution. The surface area measurements were carried out on a Quantachrome Autosorb-1 apparatus. Nitrogen adsorption/desorption isotherms were determined at -196 ˚C after degassing the sample at 150 ˚C overnight and the Brunauer–Emmett–Teller (BET) surface areas (S_{BET}) were estimated by adsorption data in a relative pressure range from 0.01 to 0.1. The X-ray photoelectron spectroscopy (XPS) measurements were performed using a Kratos Axis Ultra X-ray photoelectron spectrometer (Karatos Analytical Ltd., Manchester, UK) using an Al *Kα* monochromatic radiation source (1486.7 eV) with 90° takeoff angle (normal to analyzer). The vacuum pressure in the analyzing chamber was maintained at 2 x 10^{-9} Torr. The XPS spectra were collected for C1s, O1s, Zn2p and Co2p levels with pass energy 20 eV and step 0.1 eV. The binding energies were calibrated relative to C1*s* peak energy position as 285.0 eV. Data analyses were done using Casa XPS (Casa Software Ltd.) and Vision data processing program (Kratos Analytical Ltd.). Four-probe resistivity of the catalyst films were measured with a homemade system built by Helmholtz Zentrum, Berlin. A thin film of catalysts (400 nm thickness) was deposited on the fluorine doped tin oxide (ITO) and the resistivity on the films before and after the electrochemical measurements were measured at 10 different points and the average value was represented.

Experimental Section

Syntheses of mixed cobalt-zinc, zinc and cobalt hydroxide carbonates

In a typical synthesis of $(Zn_xCo_{1-x})_5(OH)_6(CO_3)_2$ with x = 0.34, zinc acetate dihydrate (2.17 g) and cobalt acetate tetrahydrate (5.0 g) were first dissolved in deionized water (210 mL). Ammonium sulfate (13.2g) was also dissolved separately in water (300 mL). Both solutions were slowly mixed and stirred for 2 h. A third solution containing ammonium bicarbonate (7.9 g) in water (300 mL) was added slowly to the above mixture and stirred overnight. The obtained pink precipitate was then collected by centrifugation, washed thoroughly with distilled water and absolute ethanol, and dried at 60 ˚C for 12 h.

Similarly, for the synthesis of $(Co_xZn_{1-x})_5(OH)_6(CO_3)_2$ (x =0.34), the molar ratio of the zinc acetate dihydrate and cobalt acetate tetrahydrate was reversed without changing any other parameters. In addition to the mixed cobalt zinc hydroxide carbonates, pure cobalt and zinc hydroxide carbonates were also prepared in similar way either by using zinc acetate dihydrate or cobalt acetate tetrahydrate.

Syntheses of cobalt-zinc, zinc and cobalt oxides

The as-synthesized mixed cobalt-zinc, zinc and cobalt hydroxide carbonate precursors were taken in silica crucibles and annealed to 400 ˚C at a rate of 2 °C/min in dry synthetic air (20% O_2, 80% N_2) and maintained the temperature for an additional 8 h in a tubular furnace and then cooled to ambient temperature to form $ZnCo_2O_4$, $(Co_3O_4)/(ZnO)_6$, ZnO, and Co_3O_4, respectively.

Electrochemical Oxygen Evolution Reaction (OER)

The electrochemical experiments were carried out using rotating disk electrode (RDE, Pine Instruments) setup in a standard three-electrode electrochemical glass cell. Electrode potentials were recorded using a Biologic SP-200 potentiostat at room temperature. The working electrode was a glassy-carbon (GC) disk (5 mm diameter), while a reversible hydrogen electrode (Hydroflex, Gaskatel) and platinum gauze were used as reference and counter electrode, respectively. Fresh 0.1M KOH solution acted as alkaline electrolyte and flushed for 30 min with high-purity N_2 for further measurements. Prior to film deposition, the glassy carbon electrodes were polished and cleaned in an ultrasonic bath using ultrapure water and acetone. Typically, 5 mg of catalyst powder was suspended in a mixture of ultrapure water (3.98 mL), 2-propanol (1 mL), and Nafion solution (20 μL, 5 wt% of stock solution, Sigma–Aldrich) followed by homogenization by using a horn sonicator. The catalyst ink (10 μL of the catalyst suspension) was then dispersed on the electrode and dried in air at 60 ˚C for 10 min. The loading of the glassy carbon electrode was 51 μg cm^{-2}, and during the experiments the working electrode was rotated at a rate of 1600 rpm to ensure the hydrodynamic equilibrium. The given electrode potentials were corrected for Ohmic losses as determined from potentiostatic electrochemical impedance spectroscopy (PEIS) and referenced to the reversible hydrogen electrode (RHE). Chronoamperometric experiments were performed at RT at 1.8 V vs. RHE in 0.1M KOH solution at 1600 rpm. Quasi-stationary potential-step experiments for OER activity were performed in the potential range between 1.5 and 1.67 V. At each potential step a PEIS was performed, and the corresponding current was recorded after 5 min, before increasing the potential. The number of redox active Co ions N was determined from the reductive charge q of the CVs recorded at 50 mV/s by using N=q/F with Faradays constant F = 96485 C/mol. We carefully performed these experiments by using a reference electrode freshly calibrated versus a Pt/H_2 electrode in the same electrolyte. This leads to an error of the electrode potential of ±2mV. The measurement error of the current during the quasi-stationary potential step experiments was comparably small with a maximal error of 3% at the lowest potential and less than 1% above. Therefore, we concluded that the determined difference in catalytic activity is significantly above the experimental error.

X-ray absorption spectroscopy

The X-ray absorption spectra (XANES/EXAFS/XRF) were collected at the BESSY synchrotron radiation source operated by the Helmholtz-Zentrum Berlin. The measurements were performed at the KMC1 bending-magnet beamline at 20 K in a helium-flow cryostat (Oxford-Danfysik). The incident beam energy was selected by a Si(111) double-crystal monochromator. The measurements at the cobalt and zinc K-edge were performed in transmission mode with an ionization chamber and in fluorescence mode using 13-element energy-resolving Ge detector (Canberra). The extracted spectrum was weighted by k^3 and simulated in k-space (E_0 = 6547 eV). All EXAFS simulations were performed using in-house software (SimX) after calculation of the phase functions with the FEFF program (version 8.4, self-consistent field option activated).[1,2] The data range used in the simulation of the EXAFS spectra was 20–1000 eV (3–16 $Å^{-1}$). The EXAFS simulation was optimized by a minimization of the error sum obtained by summation of the squared deviations between measured and simulated values (least-squares fit). The fit was performed using the Levenberg-Marquardt method with numerical derivatives. The error ranges of the fit parameters were estimated from the covariance matrix of the fit. Further details are given elsewhere.[3-7]

$ZnCo_2O_4$ samples for XAS experiments were prepared on glassy carbon cylinders, in analogy to the electrochemical RDE experiments. Electrochemical treatment in the OER range was conducted at 1.8 V vs. RHE for 30 min in 0.1 M KOH solutions. After removal from the electrolyte under potential control, the electrode was dried and was used for XAS measurements. Similarly, bare $ZnCo_2O_4$ electrodes were also prepared and further measured for comparison and to study the surface structure phenomenon.

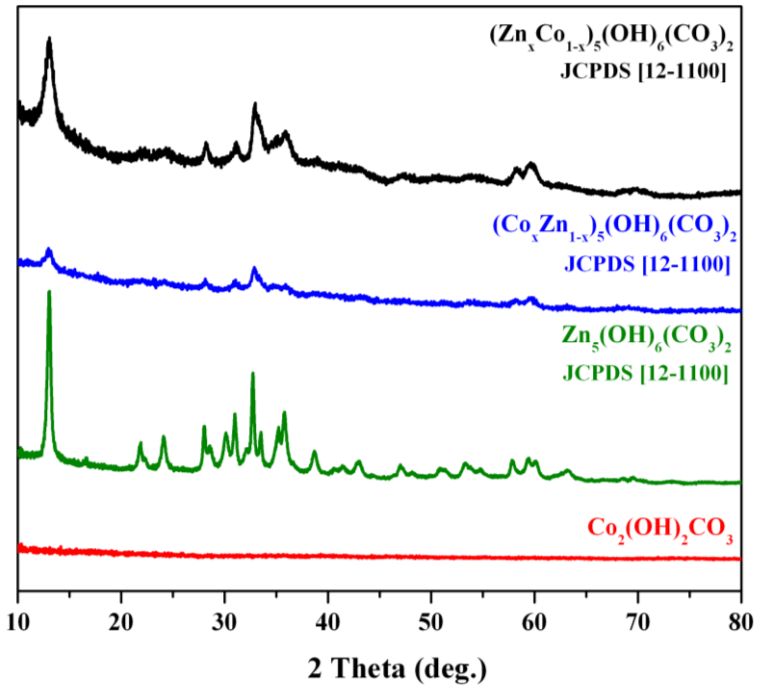

Fig. S1 PXRD of the as-prepared mixed zinc cobalt, zinc and cobalt hydroxide carbonate precursor (JCPDS 12-1100). Although the cobalt precursor was amorphous in nature, the phase identification was further carried out by IR spectroscopy and presence of hydroxide carbonate was confirmed.

Table S1. Determination of zinc and cobalt ratio in the mixed zinc cobalt hydroxide carbonate precursors as well as in cobalt zinc oxides was obtained by EDX and ICP-AES analysis. Three independent measurements were performed for the reliability and the average data is presented.

	Zn:Co (Theo.)	Zn:Co (EDX)	Zn:Co (ICP-AES)
$(Zn_{0.34}Co_{0.66})_5(OH)_6(CO_3)_2$	1:2	~0.97:2.01	1:2.05
$(Co_{0.34}Zn_{0.66})_5(OH)_6(CO_3)_2$	2:1	~2.01:0.99	1.97:1
$ZnCo_2O_4$	1:2	~1:1.98	1:2.02
$(Co_3O_4)/(ZnO)_6$	2:1	~2.04:0.97	2.03:1

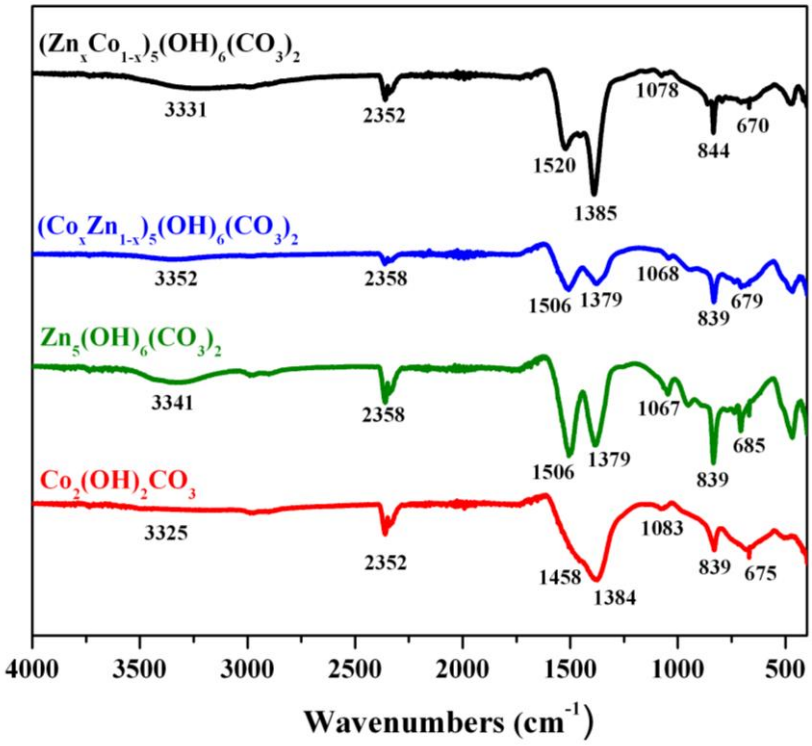

Fig. S2 FT-IR transmission spectrum of as-prepared mixed zinc-cobalt, zinc and cobalt hydroxide carbonate precursors. The sharp peaks between 670 and 844 cm^{-1} are in plane and out of plane bending vibrations of CO_3^{2-}. The bands ranging from 1379 to 1520 cm^{-1} are attributed to the asymmetric stretching mode of C–O bond whereas the weak shoulders at around 1067-1083 cm^{-1} corresponds to the symmetric C–O stretching vibration. The adsorption bands between 2352 and 2358 cm^{-1} related to the adsorbed carbon dioxide from the atmosphere during handling of samples. The peaks appearing in the range of 3325 to 3352 cm^{-1} are correlated to the O–H groups interacting with the carbonate anions in metal hydroxide carbonates. The obtained IR spectra here can be very well matched with the known zinc or cobalt hydroxide carbonates.[8-13]

Table S2. BET surface areas of as-prepared hydroxide carbonate precursors and the respective oxides.

Precursors	S_{BET} (m^2/g)	Oxides	S_{BET}(m^2/g)
$(Zn_{0.34}Co_{0.66})_5(OH)_6(CO_3)_2$	49.5	$ZnCo_2O_4$	57.0
$(Co_{0.34}Zn_{0.66})_5(OH)_6(CO_3)_2$	40.1	$(Co_3O_4)/(ZnO)_6$	42.9
$Zn_5(OH)_6(CO_3)_2$	29.2	ZnO	30.3
$Co_2(OH)_2(CO_3)_2$	42.8	Co_3O_4	38.1

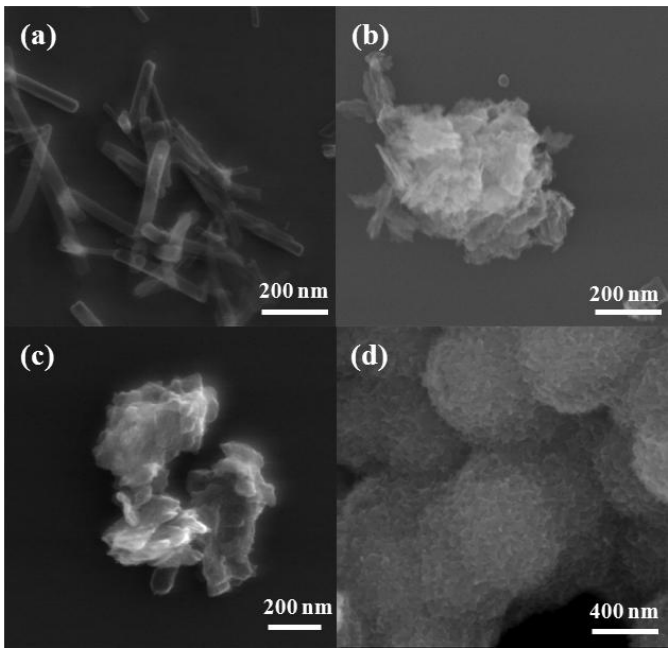

Fig. S3 The SEM micrographs of (a) rod shaped $(Zn_{0.34}Co_{0.66})_5(OH)_6(CO_3)_2$, agglomerated rods of (b) $(Co_{0.34}Zn_{0.66})_5(OH)_6(CO_3)_2$ and (c) $Zn_5(OH)_6(CO_3)_2$, and (d) spheres of $Co_2(OH)_2(CO_3)_2$.

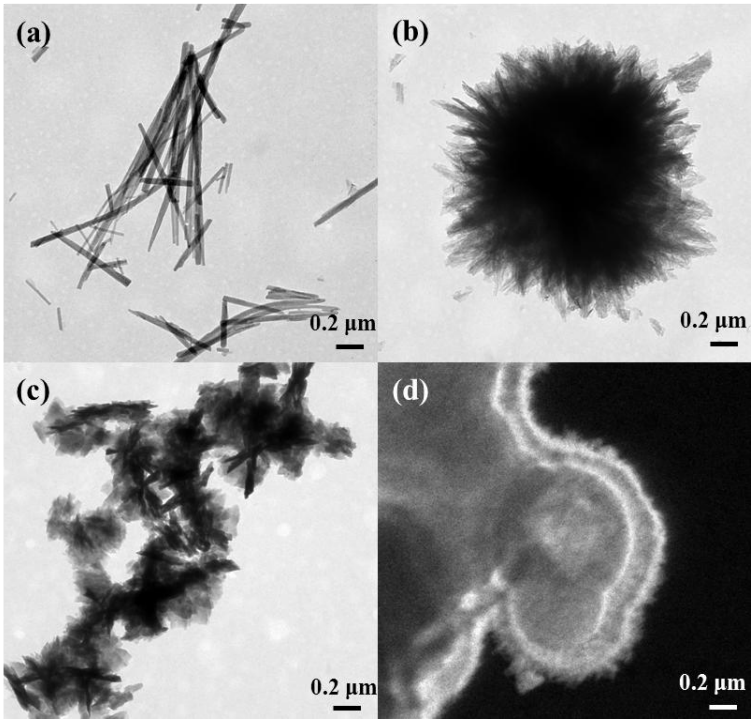

Fig. S4 The TEM micrographs of (a) $(Zn_{0.34}Co_{0.66})_5(OH)_6(CO_3)_2$, (b) $(Co_{0.34}Zn_{0.66})_5(OH)_6(CO_3)_2$, (c) $Zn_5(OH)_6(CO_3)_2$ and (d) bright field image of $Co_2(OH)_2(CO_3)_2$.

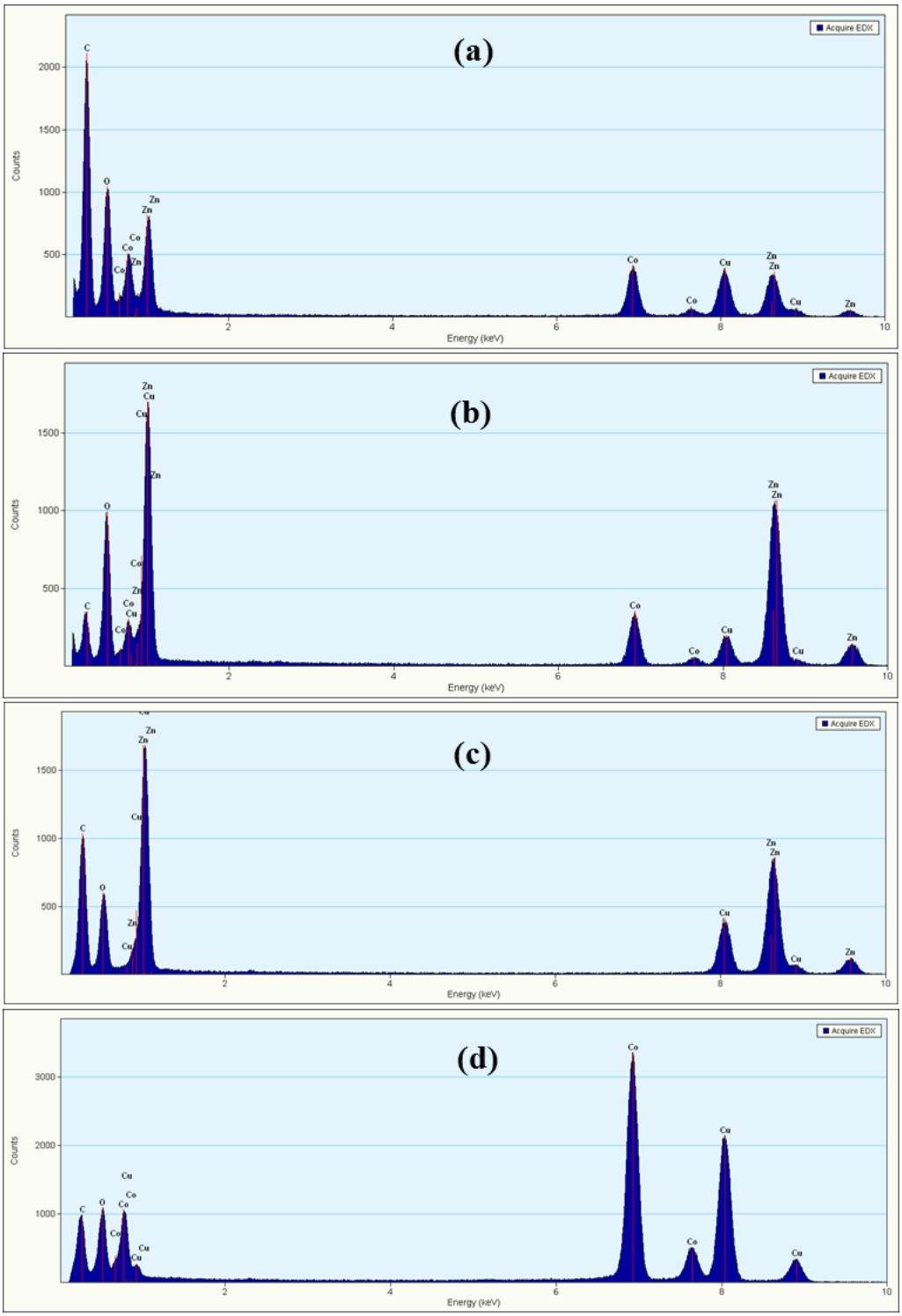

Fig. S5 The presence of zinc and cobalt in (a) $(Zn_{0.34}Co_{0.66})_5(OH)_6(CO_3)_2$, (b) $(Co_{0.34}Zn_{0.66})_5(OH)_6(CO_3)_2$, (c) $Zn_5(OH)_6(CO_3)_2$ and (d) $Co_2(OH)_2(CO_3)_2$ precursor were determined by the EDX analysis. Appearance of peaks for copper is due to TEM grid (carbon film on 300 mesh Cu-grid).

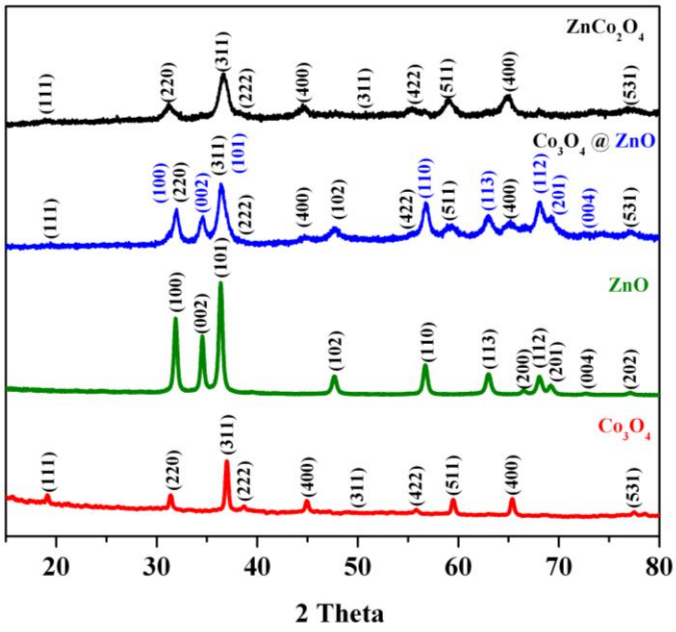

Fig. S6 PXRD (in deg) and Miller indices (hkl) of as-obtained zinc cobalt oxide ($ZnCo_2O_4$, JCPDS 23-1390), cobalt oxide at zinc oxide ($(Co_3O_4)/(ZnO)_6$, JCPDS 42-1467 and 75-576), zinc oxide (ZnO, JCPDS 75-576) and cobalt oxide (Co_3O_4, JCPDS 42-1467). In addition to the PXRD, the composition of Zn:Co was also derived from EDX and ICP-AES analysis (see Table S1).

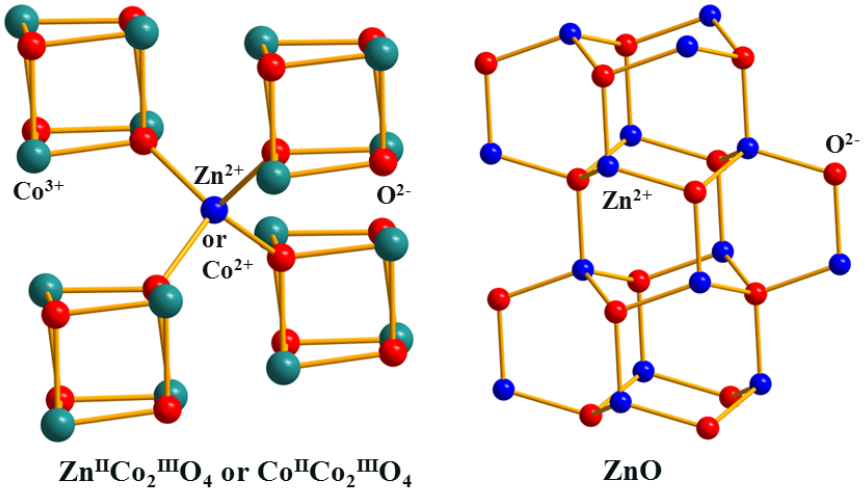

Fig. S7 The $ZnCo_2O_4$ and Co_3O_4 (left) crystallize in the cubic system with space group *Fd*3*m* (Nr. 227) and has a spinel structure ($A^{+2}B_2^{+3}O_4$). In $ZnCo_2O_4$, Zn^{2+} occupies the tetrahedral (A) sites whereas, Co^{2+} in Co_3O_4. However, the octahedral (B) sites in both structures are acquired by Co^{3+}.[14,15.] The ZnO (right) belongs to the hexagonal wurtzite system with space group P63*mc* (Nr. 186) where both zinc and oxygen are in tetrahedral coordination.[16]

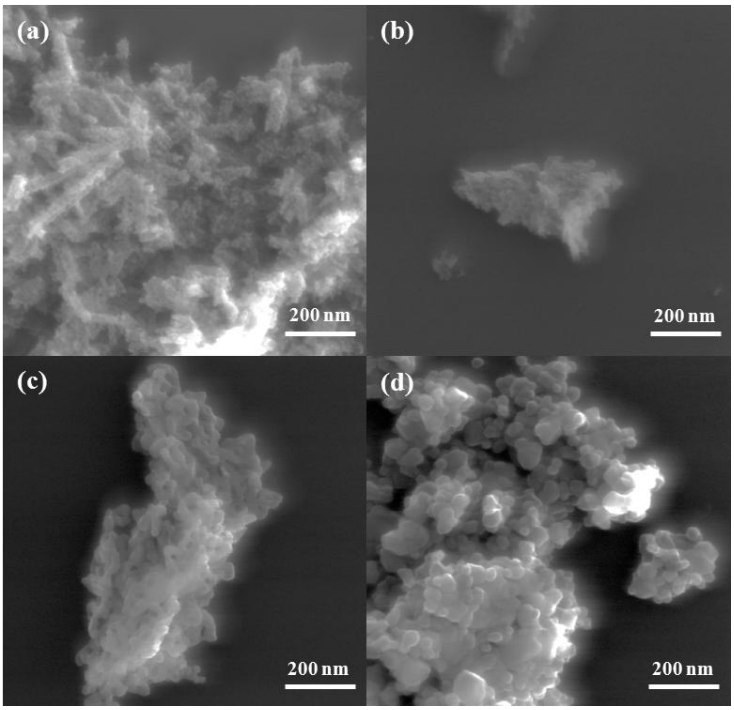

Fig. S8 SEM micrographs of (a) $ZnCo_2O_4$, (b) $(Co_3O_4)/(ZnO)_6$, (c) ZnO and (d) Co_3O_4.

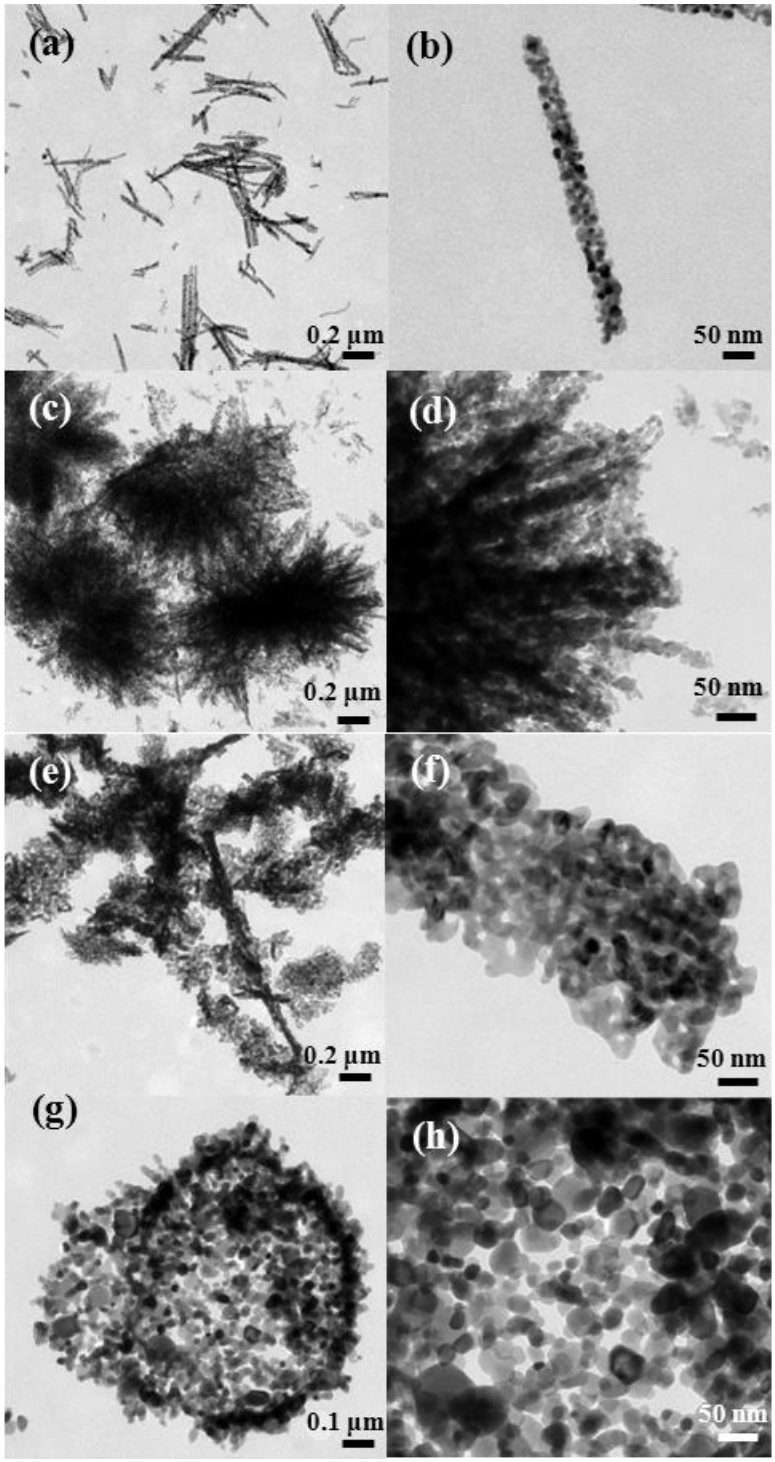

Fig. S9 The TEM images containing (a,b) nanochains of $ZnCo_2O_4$, (c,d) nanofibrous type $(Co_3O_4)/(ZnO)_6$, (e,f) nanonets of ZnO, and (g,h) spherical shaped Co_3O_4.

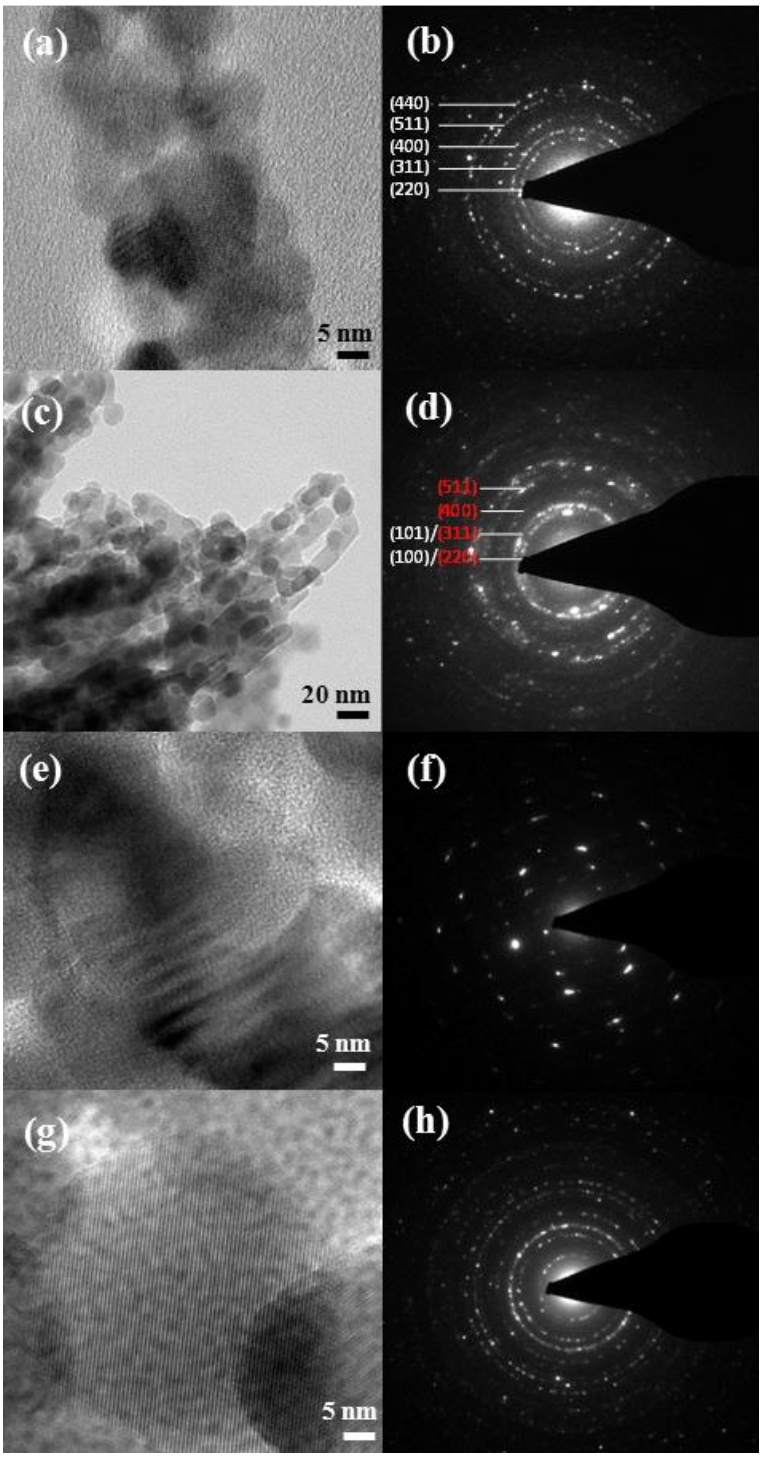

Fig. S10 The high resolution TEM images with corresponding selected-area electron diffraction patterns of (a,b) $ZnCo_2O_4$, (c,d) $(Co_3O_4)/(ZnO)_6$, (e,f) ZnO, and (g,h) Co_3O_4. The reflections of $ZnCo_2O_4$ clearly indicated the presence of a pure oxide phase whereas, indexing $(Co_3O_4)/(ZnO)_6$ reveals that the Co_3O_4 are well embedded in the ZnO structure (see b and d).

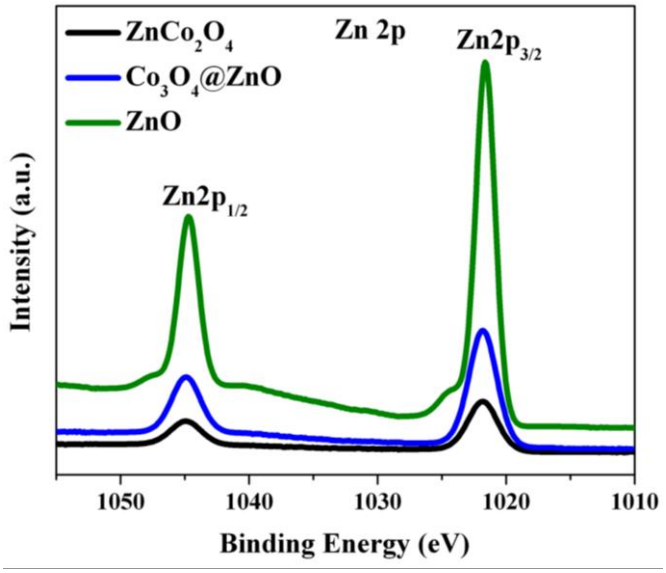

Fig. S11 The Zn2p XPS spectra of $ZnCo_2O_4$, $(Co_3O_4)/(ZnO)_6$ and ZnO. The spectra displays two peaks with binding energy values of ~1022.6 and ~1044.9 eV, which are ascribed to $Zn2p_{3/2}$ and $Zn2p_{1/2}$, indicating the Zn(II) oxidation state in the as-synthesized materials.[17] A tiny shoulder at higher binding energy can be attributed to the remnant of $ZnSO_4$ that may have formed from the starting precursor.

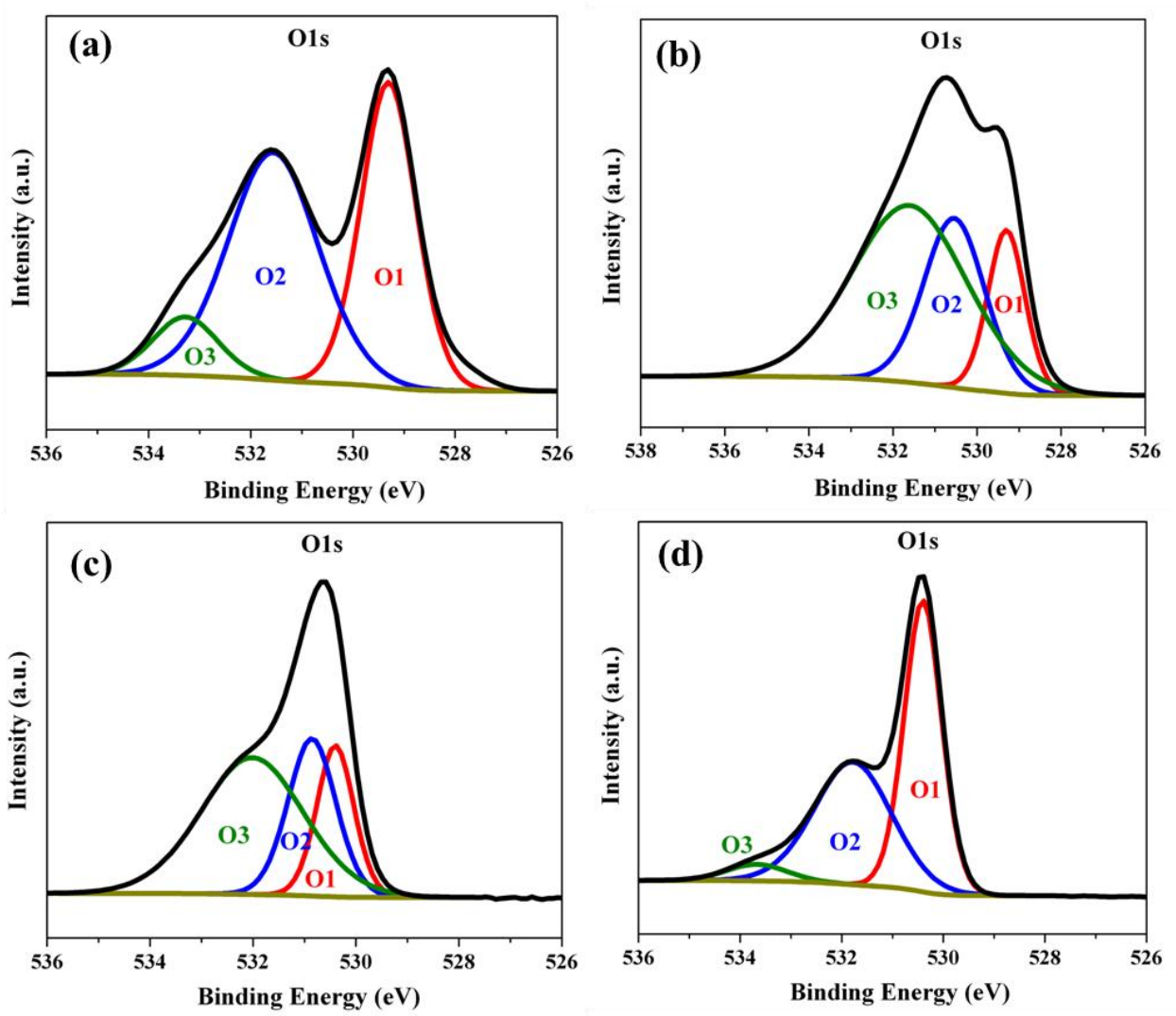

Fig. S12 The O1s XPS spectra of (a) $ZnCo_2O_4$, (b) $(Co_3O_4)/(ZnO)_6$, (c) ZnO, and (d) Co_3O_4. The O1s spectrum, in each case, was deconvoluted into three peaks (O1, O2 and O3). The peaks (O1) at ~530.0 eV correspond to metal–oxygen bonds in the metal oxide. The peaks (O2) between ~530.8 to 531.8 eV could be attributed to oxygen in –OH groups, indicating that the surface of the material is hydroxylated due to the consequence of either surface hydroxides or substitution of oxygen atoms at the surface by hydroxyl groups or the oxygen atoms of carbonate unit (C=O) as impurities from the precursors. The peaks (O3) at around 532.1 to 533.6 eV were correlated to the absorbed water molecules on the materials. The values obtained here could also be well matched with the other literature reported oxide materials.[18-24]

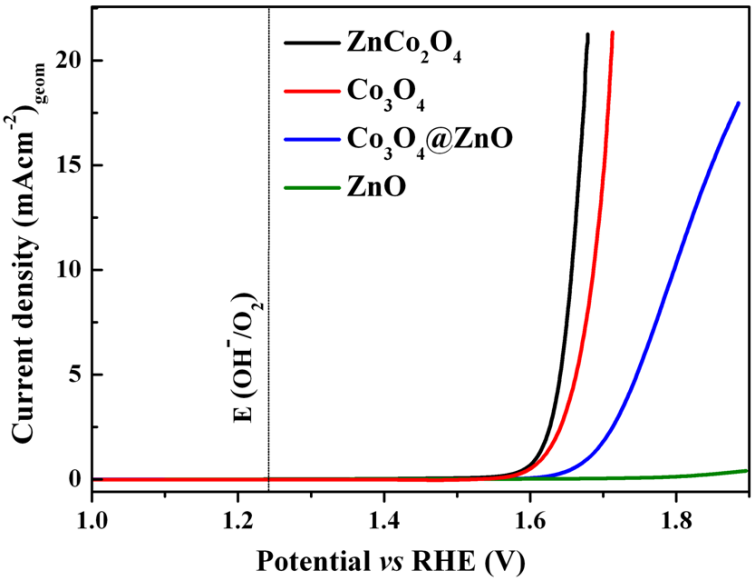

Fig. S13 Linear sweep voltammograms (LSV) of $ZnCo_2O_4$, $(Co_3O_4)/(ZnO)_6$, ZnO, and Co_3O_4 recorded in 0.1 M KOH with a sweep rate of 6 mV s^{-1} (the catalyst loading is 51 μg cm^{-2}) using a three-electrode rotating disk electrode setup.

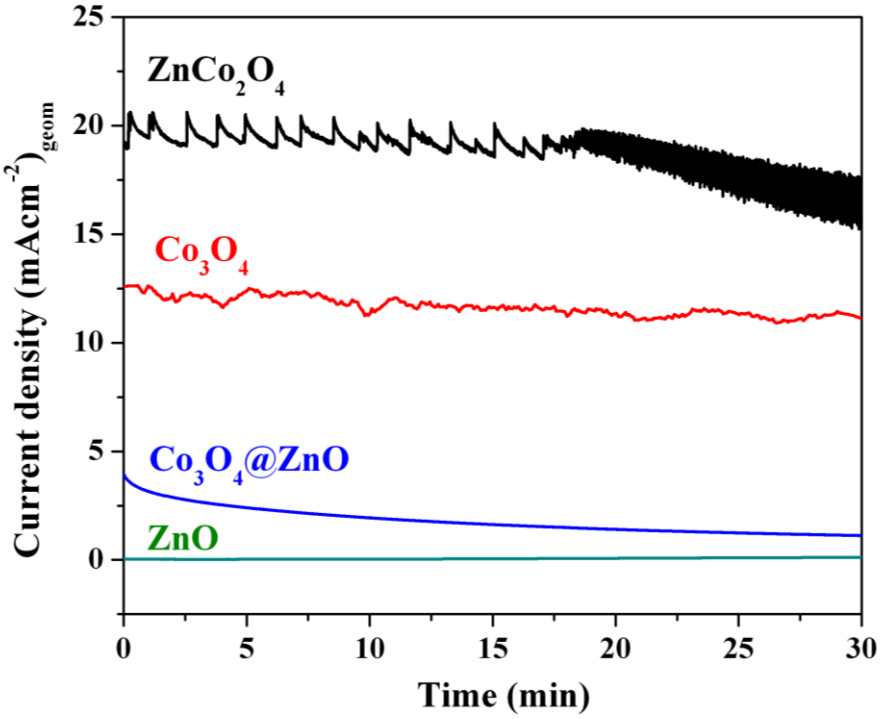

Fig. S14 Current-time chronoamperometry responses of $ZnCo_2O_4$, $(Co_3O_4)/(ZnO)_6$, ZnO, and Co_3O_4 measured at 1.8 V *vs* RHE in 0.1 M KOH solution with 1600 rpm.

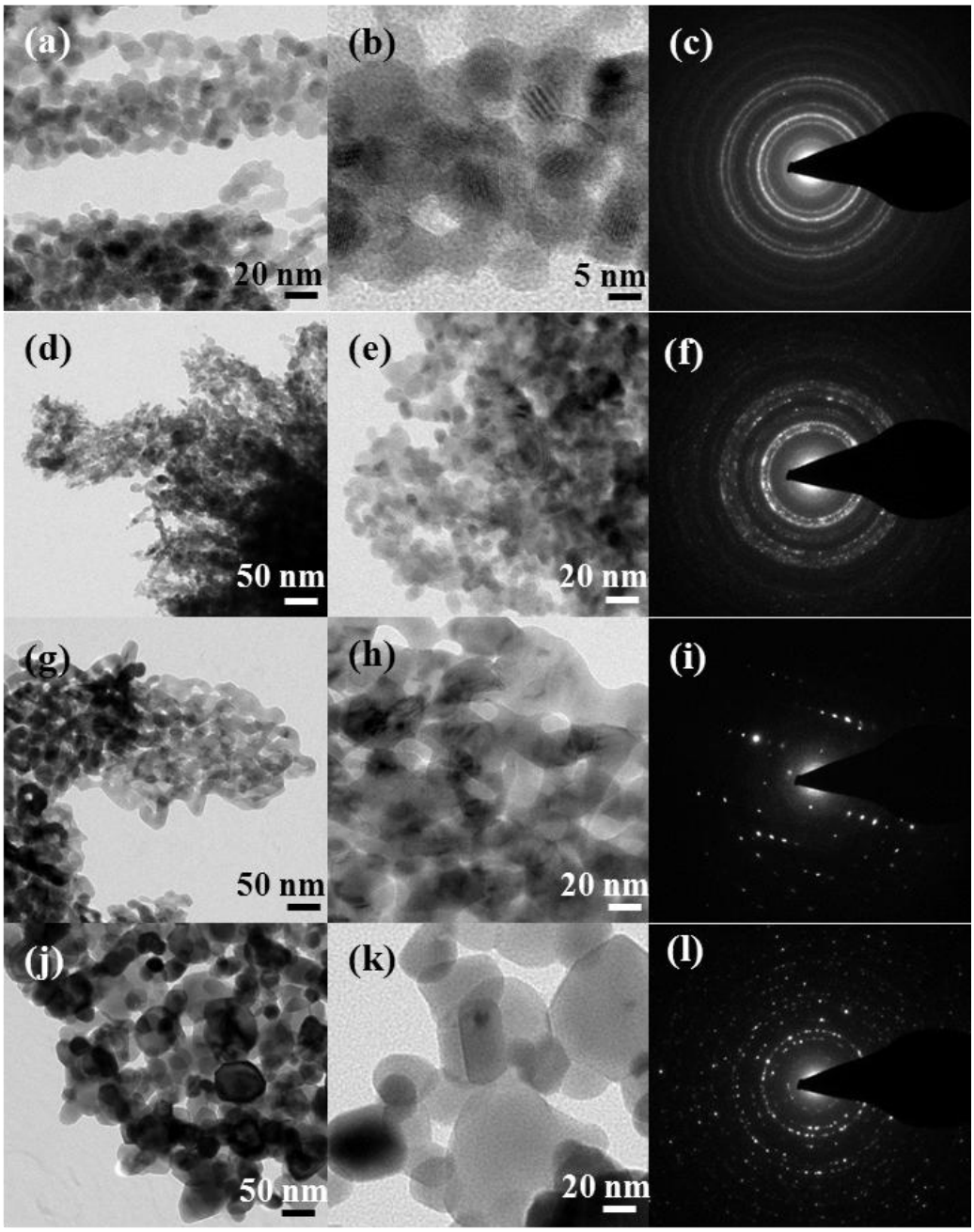

Fig. S15 The TEM, HRTEM images and SAED patterns of $ZnCo_2O_4$ (a-c), $(Co_3O_4)/(ZnO)_6$ (d-f), ZnO (g-i), and Co_3O_4 (j-l), after the current-time chronoamperometry experiments. From TEM (b, e, h, k) and SAED patterns (c, f, i, l), it could be seen that the morphology and the crystallinity of the materials are well preserved after electrocatalysis. However, having a close look at the HRTEM images (see Figure 6, main text), it appeared that the surface of materials (b, e, h) were slightly affected due to the loss of zinc in KOH (pH 13) solution (as confirmed by ICP, XPS, X-ray fluorescence emission spectra) for $ZnCo_2O_4$ and $(Co_3O_4)/(ZnO)_6$, during oxygen evolution experiments.

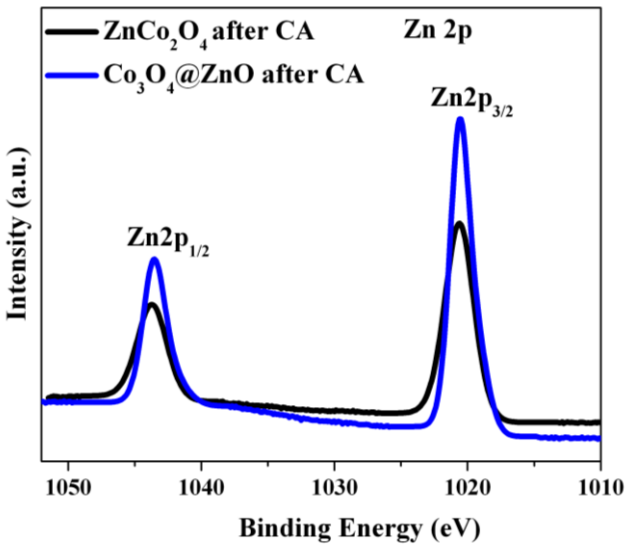

Fig. S16 The Zn2p XPS spectra of $ZnCo_2O_4$ and $(Co_3O_4)/(ZnO)_6$, after the current-time chronoamperometry. The spectra displays two peaks with binding energy values of ~1020.6 and ~1043.5 eV, corresponds to $Zn2p_{3/2}$ and $Zn2p_{1/2}$ and are consistent with the presence of Zn(II).[17]

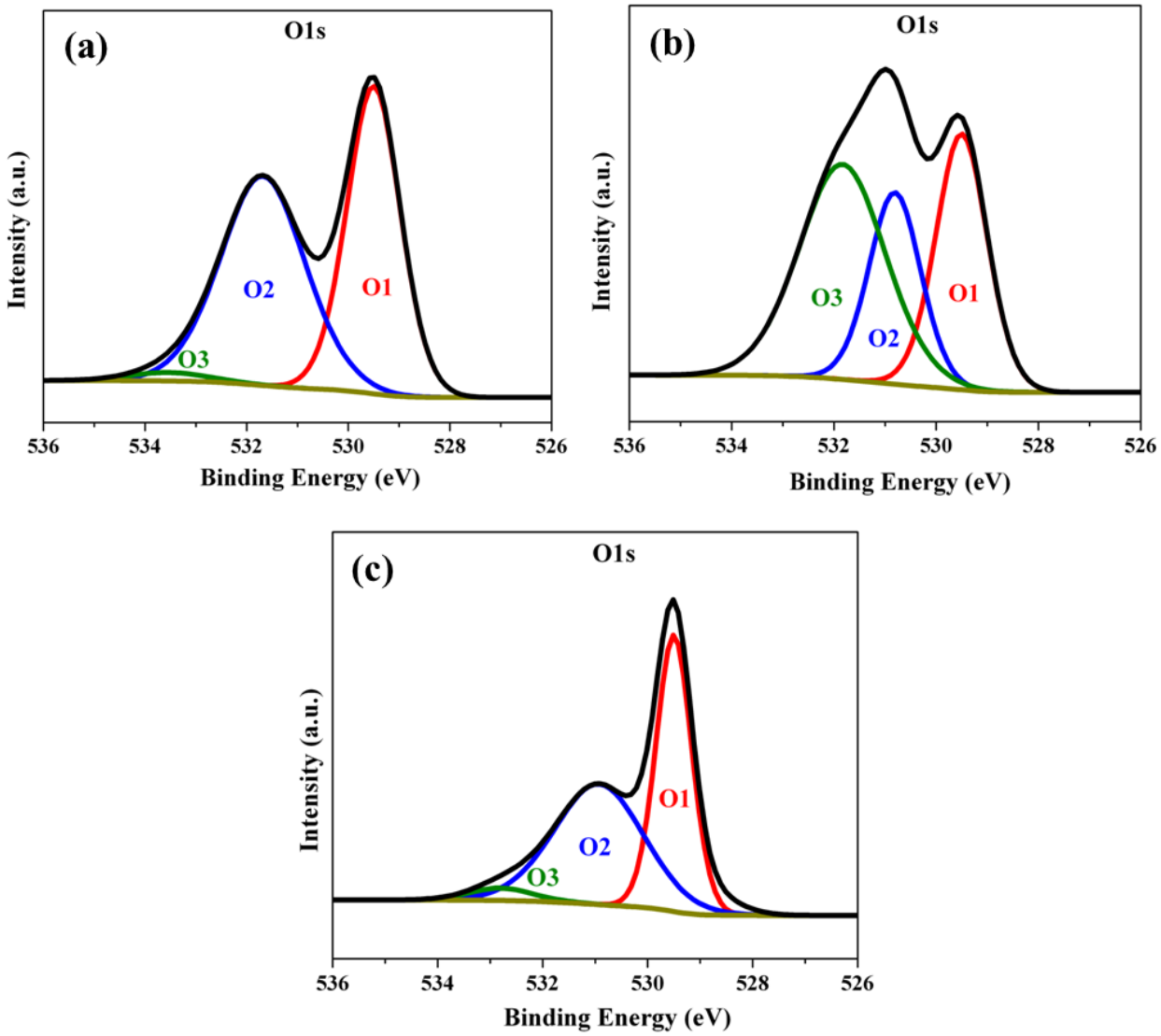

Fig. S17 The O1s XPS spectra of (a) $ZnCo_2O_4$, (b) $(Co_3O_4)/(ZnO)_6$ and (c) Co_3O_4, after the current-time chronoamperometry. The O1s spectrum in all cases was deconvoluted into three peaks (O1, O2 and O3). The peaks (O1) at ~529.8 eV correspond to metal–oxygen bonds in metal oxides. The peaks (O2) between ~530.8 to 532.5 eV were largely increased in comparison to the as synthesized oxides before electrochemical water oxidation. This shows the presence of higher fraction of –OH groups, indicating that the surface of the material is hydroxylated. The peaks (O3) at around 532.4 to 534.0 eV were correlated to the absorbed water molecules on the materials. The values obtained here is in accordance with the other literature reported oxide materials.[18-24]

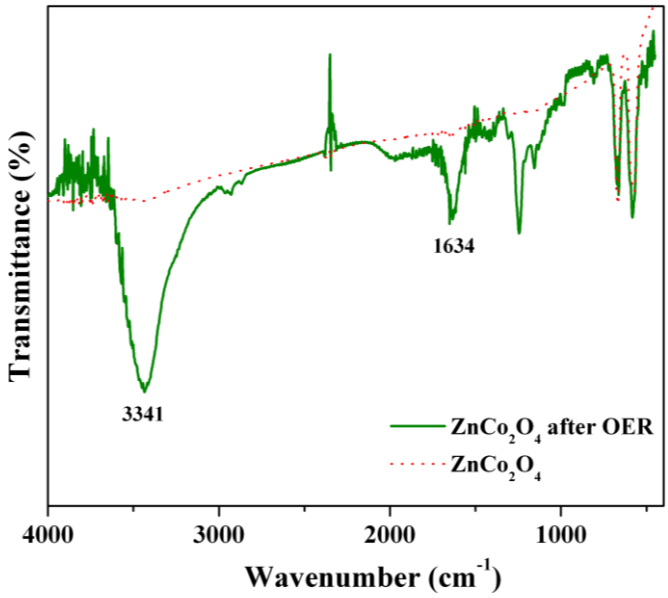

Fig. S18 FT-IR transmission spectrum of as-prepared $ZnCo_2O_4$ (red) and the $ZnCo_2O_4$ after OER experiments. The peaks at 3341 and 1634 cm^{-1} showed that the $ZnCo_2O_4$ catalyst after OER is largely hydroxylated.

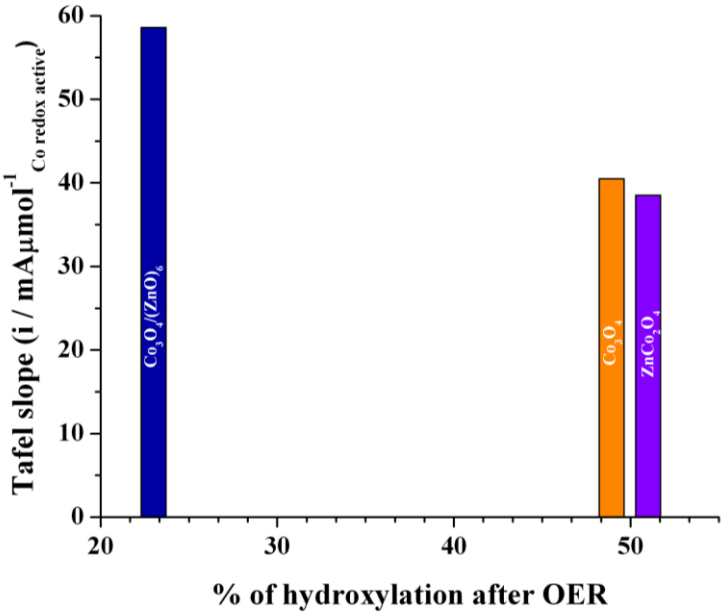

Fig. S19 The catalytic activity vs the percentage of hydroxylation plots for $ZnCo_2O_4$, $(Co_3O_4)/(ZnO)_6$ and Co_3O_4. The increase in hydroxylation is found to be beneficial for lowering of the Tafel slope.

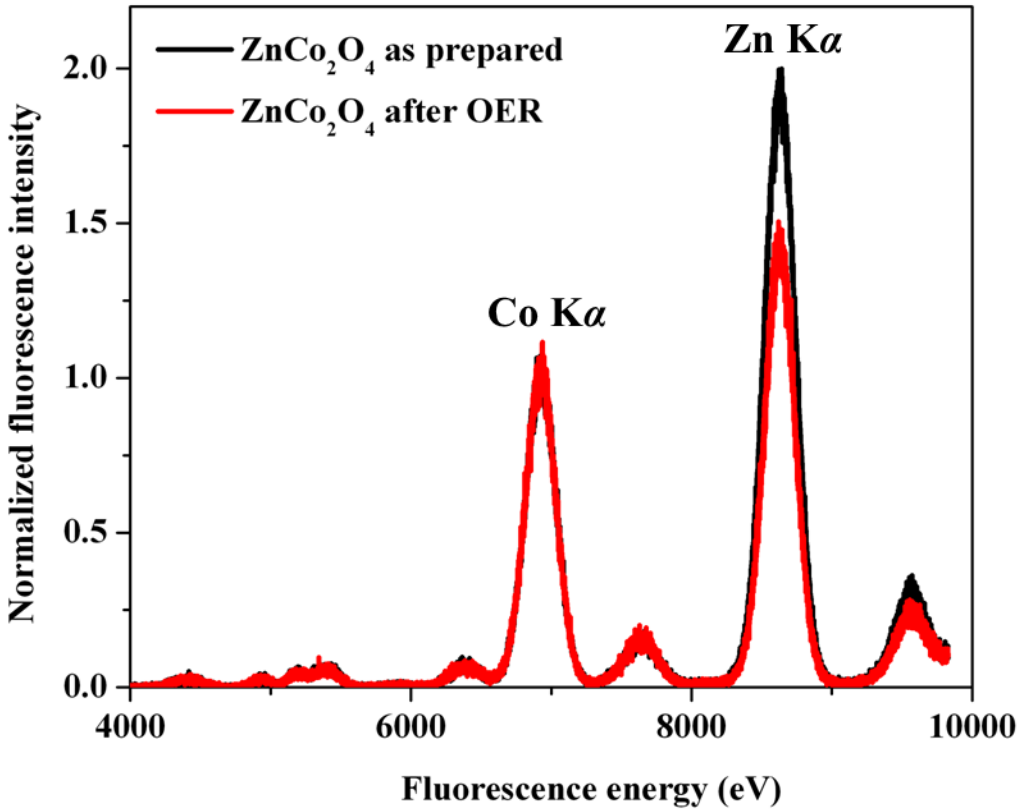

Fig. S20 X-ray fluorescence emission spectra of as prepared $ZnCo_2O_4$, after deposition on GC electrode (in black) and after operating for 30 min at 1.8 V vs. RHE in 0.1 M KOH, pH 13 (in red). The spectra shows after OER, around 25% of the Zn is lost.

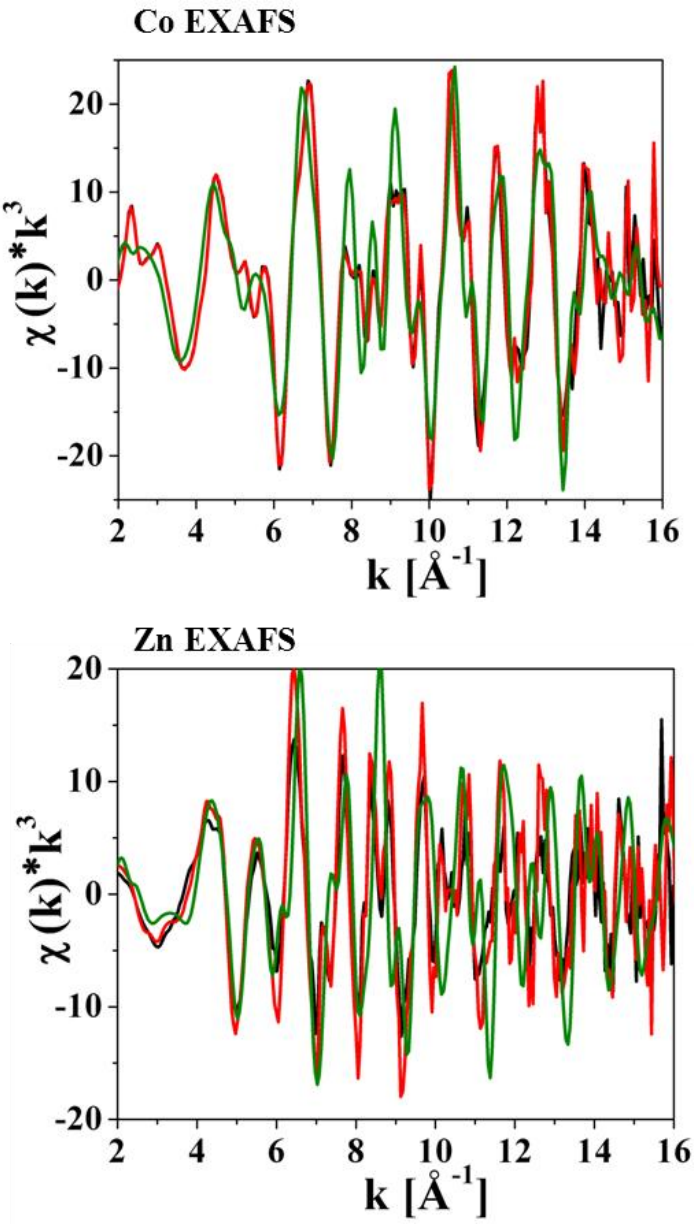

Fig. S21 k^3-weighted experimental Co and Zn EXAFS spectra of $ZnCo_2O_4$ after deposition on GC electrode (black lines), after OER experiments (red lines) and simulation results for Co in O_h sites and Zn in T_d sites of a spinel structure (green lines). The simulation parameters are given in Table S4.

Table S4. Parameters obtained by simulation (curve-fitting) of k^3-weighted EXAFS spectra of $ZnCo_2O_4$ after OER (N, coordination number; R, absorber-backscatter distance; σ, Debye-Waller parameter). Coordination numbers were fixed to values expected for Co in O_h sites and Zn in T_d sites of a spinel structure. Some distances that were common in both edges (Co-Zn distances) were fixed to the same value and were determined in a joint fit approach. Debye-Waller parameters for long-distance shells were fixed to reasonable values. Only single-scattering paths were included. Amplitude-reduction factor S_0^2 for both edges was 0.8. Fitting was performed using in-house software (SimX) after calculation of the phase functions with the FEFF program (version 8.4, self-consistent field option activated).[1,2] The error ranges of the fit parameters were estimated from the covariance matrix of the fit and represent the 68% confidence intervals[25] (error calculations as described in reference 1-7).

	Shell	Atoms	N	R (Å)	σ(Å)
Co edge	i	Co–O	6	1.896 (±0.003)	0.039 (±0.011)
	ii	Co–Co	6	2.851 (±0.002)	0.045 (±0.006)
	iii	Co–Zn	6	3.355 (±0.004)	0.063
	iv	Co–O	6	3.576 (±0.009)	0.063
	v	Co–Co	12	4.951 (±0.012)	0.063
	vi	Co–Zn	8	5.251	0.063
	vii	Co–Co	12	5.702	0.063
	viii	Co–Co	12	6.392	0.063
	ix	Co–Zn	6	6.627	0.063
	x	Co–Co	24	7.563	0.063
	xi	Co–Zn	18	7.763	0.063
Zn edge	i	Zn–O	4	1.953 (±0.012)	0.055 (±0.011)
	ii	Zn–Co	12	3.355	0.055 (±0.012)
	iii	Zn–O	12	3.395 (±0.018)	0.055
	iv	Zn–Zn	4	3.501 (±0.007)	0.055
	v	Zn–Co	16	5.251	0.055
	vi	Zn–Zn	12	5.717 (±0.007)	0.063
	vii	Zn–Co	12	6.627	0.063
	viii	Zn–Zn	12	6.704	0.063
	ix	Zn–Co	36	7.763	0.063

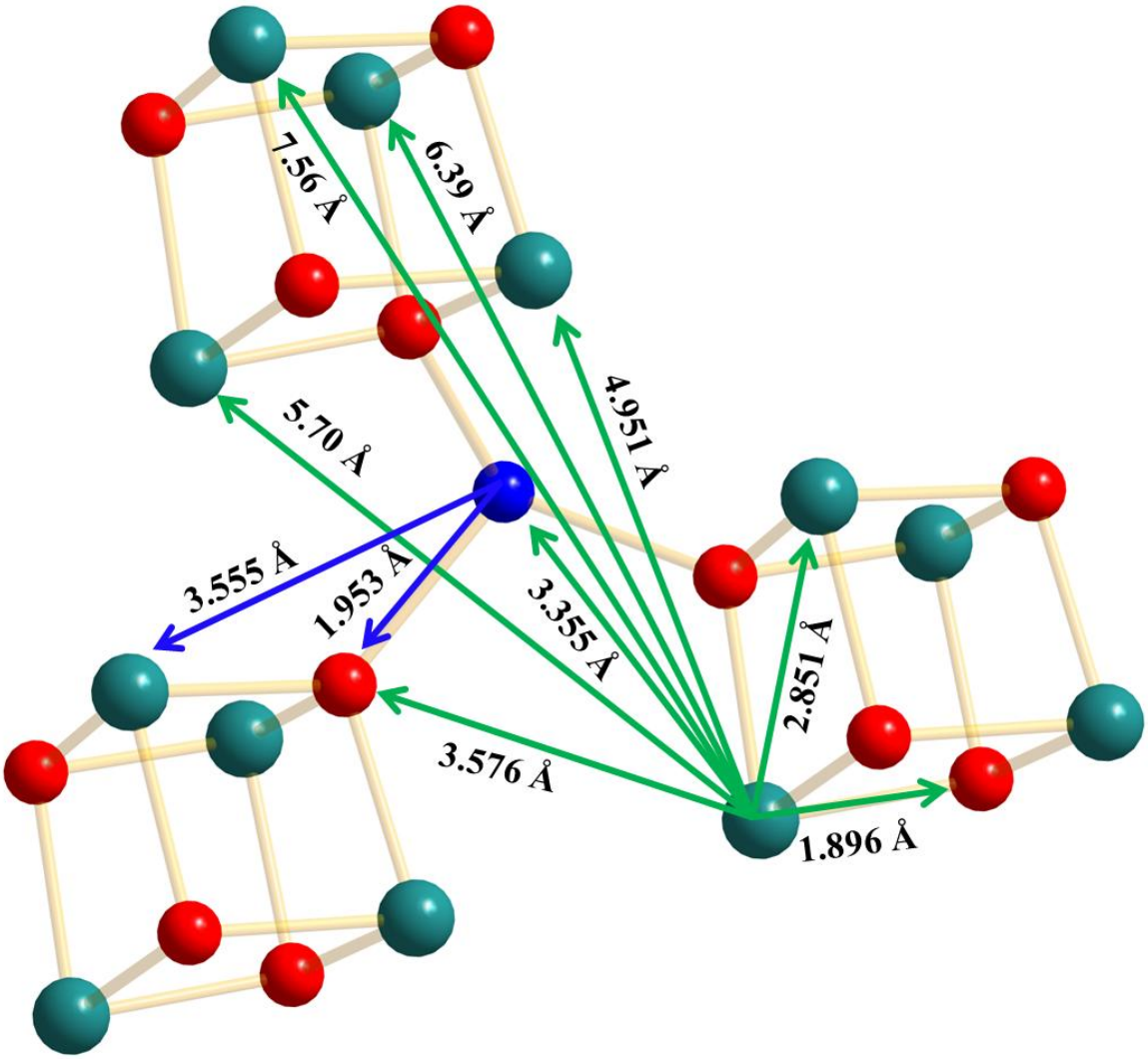

Fig. S22 Structural fragments and the reduced distances derived from EXAFS spectra of $ZnCo_2O_4$ (see Table S4 and main text for more information).

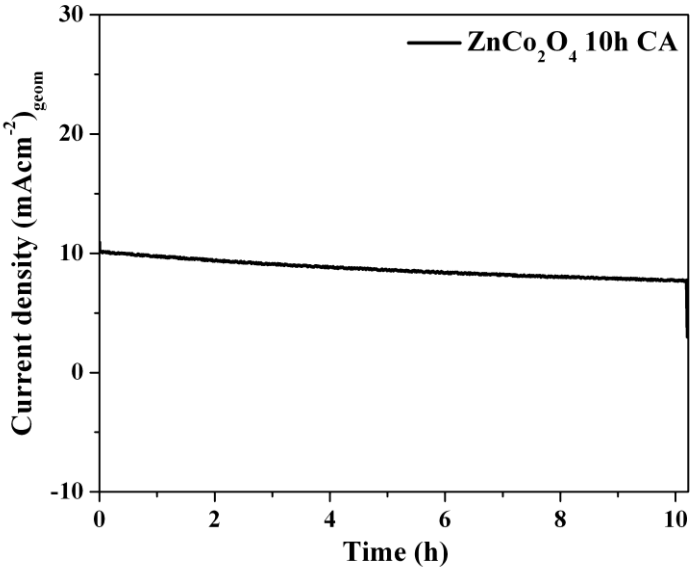

Fig. S23 Current-time chronoamperometry test for $ZnCo_2O_4$ showing about 20% decrease in current density after 10 hours of measurement at 1.65 V *vs* RHE in 0.1 M KOH solution. The degradation of OER activity could be attributed partly to the mechanical instability as well as catalytic deactivation.

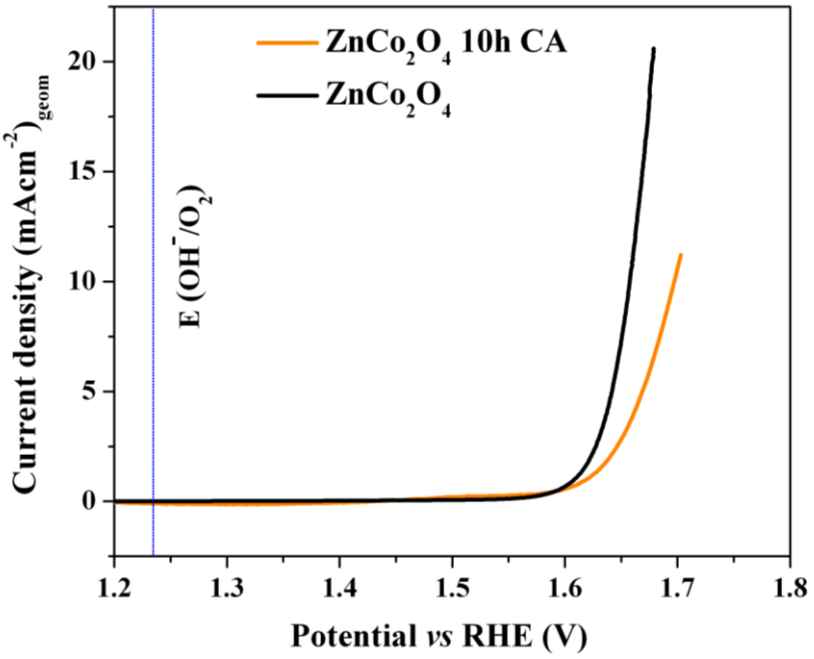

Fig. S24 Linear sweep voltammograms (LSV) of $ZnCo_2O_4$ after 10 h stability test.

References

(1) Ankudinov, A. L.; Ravel, B.; Rehr, J. J.; Conradson, S. D. *Phys. Rev. B: Condens. Mater.* **1998**, *58*, 7565-7576.

(2) Rehr, J. J.; Albers, R. C. *Rev. Mod. Phys.* **2000**, *72*, 621-654.

(3) Bergmann, A.; Zaharieva, I.; Dau, H.; Strasser, P. *Energy Environ. Sci.* **2013**, *6*, 2745-2755.

(4) Risch, M.; Khare, V.; Zaharieva, I.; Gerencser, L.; Chernev, P.; Dau, H. *J. Am. Chem. Soc.* **2009**, *131*, 6936-6937.

(5) Risch, M.; Klingan, K.; Ringleb, F.; Chernev, P.; Zaharieva, I.; Fischer, A.; Dau, H. *ChemSusChem* **2012**, *5*, 542-549.

(6) Zaharieva, I.; Chernev, P.; Risch, M.; Klingan, K.; Kohlhoff, M.; Fischer, A.; Dau, H. *Energy Environ. Sci.* **2012**, *5*, 7081-7089.

(7) Wiechen, M.; Zaharieva, I.; Dau, H.; Kurz, P. *Chem. Sci.* **2012**, *3*, 2330-2339.

(8) Sreedhar, B.; Vani, C.; Devi, D. K.; Rao, M. V. B.; Rambabu, C. *Am. J. Mat. Sci* **2012**, *2*, 5-13.

(9) Japic, D.; Bitenc, M.; Marinsek, M.; Orel, Z. C. *Mater. Res. Bull., 2014, 60*, 738-745.

(10) Nassar, M. Y.; Ahmed, I. S. *Polyhedron*, **2011**, *30*, 2431-2437.

(11) Huang, C. K.; Kerr, P. F. *Am. Mineral.* **1960**, *45*, 311-324.

(12) Wang, L.; Tang, F.; Ozawa, K.; Chen, Z.-G.; Mukherj, A.; Zhu, Y.; Zou, J.; Cheng, H.-M.; Lu, G. Q. *Angew. Chem. Int. Ed.* **2009**, *48*, 7048-7051.

(13) Yang, J.; Cheng, H.; Frost, R. L. *Spectrochimica Acta Part a-Molecular and Biomolecular Spectroscopy*, **2011**, *78*, 420-428.

(14) Roth, W. L. *J. Phys. Chem. Solids* **1964**, *25*, 1-10.

(15) Krezhov, K.; Konstantinov, P. *J. Phys. Condens. Matter* **1993**, *5*, 9287-9294.

(16) Abrahams, S. C.; Bernstein, J. L. *Acta Crystallogr. B* **1969**, *B25*, 1233-6.

(17) Hu, L. L.; Qu, B. H.; Li, C. C.; Chen, Y. J.; Mei, L.; Lei, D. N.; Chen, L. B.; Li, Q. H.; Wang, T. H. *J. Mater. Chem. A* **2013**, *1*, 5596-5602.

(18) Prabu, M.; Ketpang, K.; Shanmugam, S. *Nanoscale*, **2014**, *6*, 3173-3181.

(19) Tian, Z.-Y.; Ngamou, P. H. T.; Vannier, V.; Kohse-Hoeinghaus, K.; Bahlawane, N. *Appl. Catal. B*, **2012**, *117*, 125-134.

(20) Tan, B. J.; Klabunde, K. J.; Sherwood, P. M. A. *J. Am. Chem. Soc.* **1991**, *113*, 855-861.

(21) Ma, S.; Sun, L.; Cong, L.; Gao, X.; Yao, C.; Guo, X.; Tai, L.; Mei, P.; Zeng, Y.; Xie, H.; Wang, R. *J. Phys. Chem. C* **2013**, *117*, 25890-25897.

(22) Li, J.; Wang, J.; Liang, X.; Zhang, Z.; Liu, H.; Qian, Y.; Xiong, S. *ACS Appl. Mater. Interfaces* **2014**, *6*, 24-30.

(23) Menezes, P. W.; Indra, A.; Gonzalez-Flores, D.; Sahraie, N. R.; Zaharieva, I.; Schwarze, M.; Strasser, P.; Dau, H.; Driess, M. *ACS Catal.* **2015**, *5*, 2017-2027.

(24) Menezes, P. W.; Indra, A.; Sahraie, N. R.; Bergmann, A.; Strasser, P.; Driess, M. *ChemSusChem* **2015**, *8*, 164-171.

(25) Risch, M.; Klingan, K.; Heidkamp, J.; Ehrenberg, D.; Chernev, P.; Zaharieva, I.; Dau, H. **2011**, *Chem. Commun., 47*, 11912-11914.